Realization of a spin-$\frac{1}{2}$ spatially anisotropic square lattice in a quasi-two-dimensional quantum antiferromagnet $Cu(en)(H_2O)_2SO_4$

L. Lederová,[1] A. Orendáčová,[1,*] J. Chovan,[2] J. Strečka,[1] T. Verkholyak,[3] R. Tarasenko,[1] D. Legut,[4] R. Sýkora,[4] E. Čižmár,[1] V. Tkáč,[1] M. Orendáč,[1] and A. Feher[1]

[1]*Centre of Low Temperature Physics of SAS and Institute of Physics, P. J. Šafárik University, Park Angelinum 9, 040 00 Košice, Slovakia*

[2]*Department of Physics, Matej Bel University, Tajovského 40, 974 01 Banská Bystrica, Slovakia*

[3]*Institute for Condensed Matter Physics, NASU, 1 Svientsitskii Street, 790 11 Lviv, Ukraine*

[4]*ITI4 Innovation Center, Technical University of Ostrava, 17.Listopadu, 708 33 Ostrava, Czech Republic*

(Received 8 November 2016; revised manuscript received 10 February 2017; published 28 February 2017)

Theoretical and experimental studies of a quasi-two-dimensional quantum antiferromagnet $Cu(en)(H_2O)_2SO_4$ ($en = C_2H_8N_2$) were performed. *ab initio* calculations of exchange interactions confirmed that the system represents a realization of a spatially anisotropic zigzag square lattice. Corresponding quantum Monte Carlo calculations of thermodynamic quantities were realized and the results were applied in the analysis of experimental susceptibility, magnetization, and specific heat studied at temperatures ranging from nominally 300 mK up to 8 K and magnetic fields up to 14 T. The analysis of experimental results provided the estimates of intralayer exchange couplings, $J/k_B = 3.5 \pm 0.2$ K and $J' = 0.35J$. Theoretical analysis of spin symmetries in $Cu(en)(H_2O)_2SO_4$ structure predicted the presence of symmetric exchange anisotropies (out-of plane and in-plane spin anisotropy) and a spin-flop transition within the easy plane induced by the magnetic field applied along the easy axis. Isothermal magnetization measurements indicated the expected transition in the field 200 mT applied along the *b* axis which was finally identified as the easy axis lying within the easy plane *bc*. Magnetic phase diagrams with saturation fields about 6.5 T show nearly identical behavior in all studied directions. Differences appear only in weak magnetic fields as a result of the presence of weak exchange anisotropies $\approx 10^{-3}J$. The present analysis suggests that $Cu(en)(H_2O)_2SO_4$ can be a model system for exploring the interplay of quantum fluctuations, exchange anisotropies, and magnetic field in the two-dimensional lattice space.

DOI: 10.1103/PhysRevB.95.054436

I. INTRODUCTION

Considerable theoretical effort has been devoted to understanding of low-dimensional quantum magnets as examples of strongly interacting quantum many-body systems. The two-dimensional (2D) model of spin-$\frac{1}{2}$ Heisenberg antiferromagnet on the square lattice represents an important paradigm of a low-dimensional magnetism [1,2]. Depending on the sort of the spatial anisotropy of exchange coupling within a layer, many variations have been derived from this simple model, involving dimerized and frustrated lattices [1,3,4].

A model of the spatially anisotropic Heisenberg antiferromagnetic (HAF) square lattice with the nearest-neighbor coupling [Fig. 1(a)] described by the Hamiltonian [5]

$$H = \sum_{i,j} [J(\boldsymbol{S}_{i,j} \cdot \boldsymbol{S}_{i+1,j}) + J'(\boldsymbol{S}_{i,j} \cdot \boldsymbol{S}_{i,j+1})] \qquad (1)$$

represents the simplest way of introducing the spatial anisotropy of exchange coupling. $\mathbf{S}_{i,j}$ denotes a spin operator at site i of chain j. J and J' denote intrachain and interchain coupling, respectively. The model interpolates between the chain ($R = J'/J = 0$) and the spatially isotropic square lattice ($R = 1$). Theoretical investigations [5] of a staggered magnetization N in the ground state of the model (1) found that a minute amount of the interchain coupling leads to the ordered ground state with $N \sim \sqrt{J'/J}$. The small N grows with decreasing spatial anisotropy $(1 - R)$, where $R \to 1$, quickly achieving its maximal value $N \approx 0.3$ already for $R \approx 0.5$ [6–9].

The properties of the spatially isotropic square lattice have been intensively theoretically investigated, involving plethora effects as various kinds of exchange anisotropy, magnetic fields, and interlayer coupling [2,10–17]. On the other hand, the aforementioned spatially anisotropic analog with $R < 1$ has not received so much attention. The lack of corresponding theoretical predictions and difficulties with preparation of such materials did not allow finding proper experimental realizations of the HAF square lattice with $R < 1$. A few spin-$\frac{1}{2}$ systems appeared only recently. A tiny spatial anisotropy of exchange coupling within a magnetic layer was indicated in the underdoped cuprate superconductor $YBa_2Cu_3O_{6.45}$ [18]. Numerical simulations of susceptibility and magnetization in the whole range of R enabled the identification of the spatial anisotropy in quasi-2D Cu(II) based magnetic insulators $Cu(pz)Cl_2$ (pz=pyrazine) with $R = 0.3$ and $J/k_B = 8$ K, $Cu(pz)(N_3)_2$ with $R \approx 0.5$ and $J/k_B = 15$ K and $Cu(2\text{-apm})Cl_2$ (2-apm = 2-aminopyrimidine) with $R \approx 0.08$ and $J/k_B = 116$ K [19]. Rather weak spatial anisotropy was found in other quasi-2D antiferromagnet $Cu(PM)(EA)_2$ (PM = anion of pyromellitic acid, EA = ethylamine) with $R = 0.7$ and $J/k_B = 8$ K [20].

$Cu(en)(H_2O)_2SO_4$ (en=ethylendiamine) (CUEN) was originally identified as a quasi-2D representative of a spin-$\frac{1}{2}$ HAF spatially anisotropic triangular lattice from the Néel phase which is characterized by pronounced square-lattice features and ordered ground state [21]. The size of the effective intralayer coupling was estimated $J_{\text{eff}}/k_B = 2.8$ K. Recent

*alzbeta.orendacova@upjs.sk

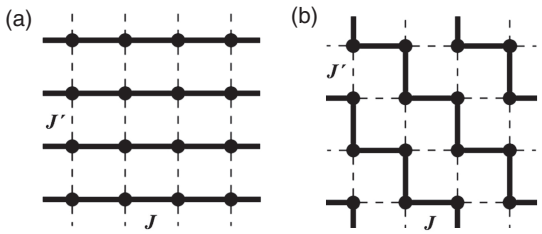

FIG. 1. (a) Spatially anisotropic square lattice. (b) Spatially anisotropic zigzag square lattice.

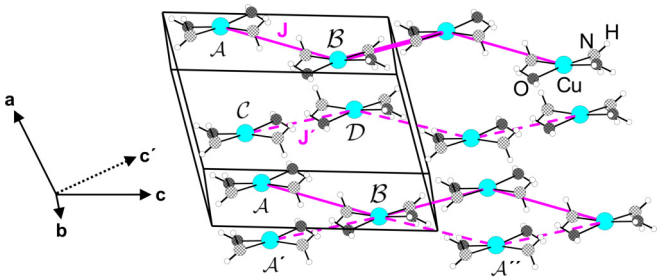

FIG. 2. Crystal structure of CUEN. Carbon atoms and $[SO_4]^{2-}$ anions are omitted for clarity. The latter connect Cu atoms with the same label, forming covalent chains along the a axis. Cu atoms denoted as $\mathcal{A}$, $\mathcal{B}$, $\mathcal{A}'$, and $\mathcal{A}''$ lie within the bc plane. The axis c' lies in the ac plane and is orthogonal to a and b axes. In accord with the quotation in Fig. 1, the strongest antiferromagnetic exchange interactions found by *ab initio* studies [22] are also depicted.

ab initio calculations [22] showed that a magnetic subsystem of CUEN can be treated as a 2D array of coupled HAF chains forming a spatially anisotropic zigzag square lattice with $R \approx 0.15$ [Fig. 1(b)]. While in zero magnetic field, a phase transition to magnetic long-range order was observed at the temperature $T_N = 0.91 \pm 0.02$ K, the application of magnetic field along the a axis increased transition temperatures. A corresponding magnetic phase diagram possesses features characteristic for a magnetic-field-induced Berezinskii-Kosterlitz-Thouless phase transition [23]. The analysis of electron paramagnetic resonance (EPR) spectra [24] revealed the presence of the weak exchange anisotropy $\approx 10^{-3} J_{\text{eff}}$.

Previous analysis of CUEN data could grasp only main features of magnetism in CUEN due to the absence of theoretical predictions involving the exchange anisotropy as well as the spatial anisotropy of the square lattice. Therefore, one of the goals of this work is devoted to the numerical studies of the model of HAF spatially anisotropic zigzag square lattice with spin $\frac{1}{2}$. Another goal is the theoretical study of the exchange anisotropy and spatial anisotropy of exchange coupling in CUEN. The results are applied in the analysis of experimental data to show that CUEN due to its simplicity represents a model system of the spin-$\frac{1}{2}$ spatially anisotropic HAF zigzag square lattice with extremely weak exchange anisotropy.

This paper is organized as follows. A synthesis procedure and experimental details are described in Sec. II. Section III involves *ab initio* calculations of exchange interactions in CUEN, quantum Monte Carlo simulations of magnetic properties of the spatially anisotropic zigzag square lattice, and symmetry analysis of spin interactions in CUEN. In Sec. IV, the theoretical results are applied for the analysis of the specific heat, magnetization, and susceptibility data as well as for the interpretation of experimental magnetic phase diagrams studied in the wide interval of magnetic fields. The impact of the exchange anisotropy and the spatial anisotropy within magnetic layer on the occurrence of a field-induced 2D Ising and Berezinskii-Kosterlitz-Thouless phase transition is discussed.

II. EXPERIMENTAL DETAILS

The crystal structure of CUEN determined at 300 K is monoclinic, space group $C2/c$ with the unit-cell parameters $a = 7.232$ Å, $b = 11.725$ Å, and $c = 9.768$ Å with the monoclinic angle $\beta = 105.5°$, and $Z = 4$. The structure (Fig. 2) consists of neutral covalent chains running along the crystallographic a axis which are linked by hydrogen bonds along the b and c axes [25]. Cu(II) ions are located in the center of O_4N_2 octahedrons which are strongly elongated along the a axis; the average bond lengths within the equatorial plane do not exceed 1.98 Å and the bond lengths between Cu and O in the apical positions are about 2.5 Å. In Fig. 2, the apical positions are omitted for clarity. Note that equatorial plane of the octahedron is parallel with the bc^* plane. The analysis of the powder neutron diffraction patterns of the deuterated analog d-CUEN confirmed the preservation of the monoclinic space group $C2/c$ symmetry at least down to 0.4 K [24]. Using a modified method [25], single crystals of CUEN were prepared in the form of blue elongated plates with typical dimensions $a' \times b' \times c' = 15 \times 0.5 \times 3$ mm^3. The a and b axes coincide with the a' and b' edges, respectively. The c axis lies within the $a'c'$ plane, tilting from the c' edge by the angle $\approx 15°$. We note that the c' direction is parallel with c^*.

Magnetization and static-susceptibility measurements were performed in a commercial Quantum Design Superconducting Quantum Interference Device (SQUID) magnetometer with a 3He insert. A sample with a mass of 60 mg was used for the bulk measurements. Using standard Pascal constants, the susceptibility data were corrected for the core diamagnetism.

Specific-heat measurements of a sample with a mass of 1 mg were performed over the temperature range from 350 mK to 4 K in the magnetic field ($B \equiv \mu_0 H$), up to 14 T in a commercial Quantum Design Physical Property Measurements System equipped with a 3He insert. The contribution of the background addenda was determined in separate runs.

III. CALCULATIONS

A. Spatial anisotropy of exchange couplings in CUEN

1. First-principle calculations

The *ab initio* studies are focused at the calculation of magnetic interactions to test a low-dimensional character of magnetic correlations in CUEN as proposed in Ref. [22]. Present calculations used similar technique, i.e., the spin-polarized density-functional theory (DFT) method implementing the projector-augmented wave formalism [26] with the generalized gradient approximation (GGA) as parametrized by Perdew, Burke, and Ernzerhof [27] to treat the exchange

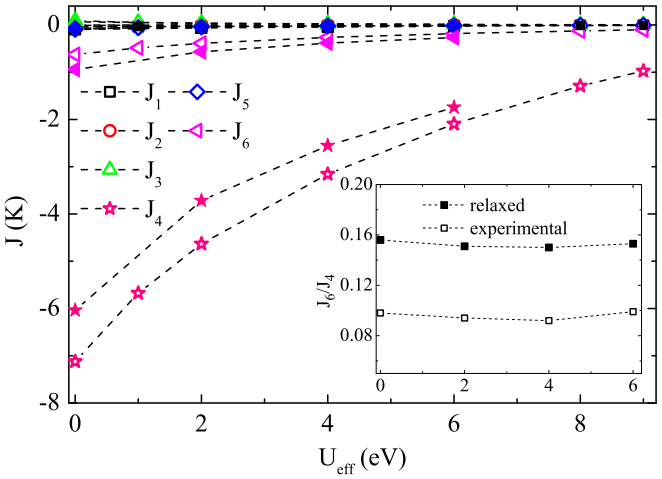

FIG. 3. Dependence of exchange coupling parameters (corresponding to the Hamiltonian introduced in Ref. [22]) on U_{eff} values. Full and empty symbols represent J values calculated from relaxed [22] and experimental structural parameters, respectively. Inset: ratio J_6/J_4 vs U_{eff} values.

correlation effects. Additionally, the onsite Coulomb repulsion interaction is considered within the rotationally invariant form of GGA+U approach [28], where the localized $3d$ electrons experience a spin- and orbital-dependent potential (U) and the exchange interaction J, while the other orbitals are delocalized and treated by the conventional GGA. The localization/itineracy of the $3d$ electrons on copper atoms is controlled by changing the value of U and keeping the value of J constant, i.e., using rather $U_{\text{eff}} = (U - J)$. The Brillouin zone integration is performed with the reduced k points $6 \times 4 \times 5$ and the Kohn-Sham wave functions are expanded into plane waves up to a cutoff energy of 500 eV. In accord with the previous studies [22], we considered 14 Cu neighbors coupled by $J_1, J_2, \ldots, J_6$ exchange coupling parameters (Figs. 1 and 3 in Ref. [22]). The first nonincluded Cu atoms were in the distance larger than 9.7 Å from the central Cu atom.

While previous calculations [22] used relaxed lattice parameters and atomic positions, in this study, experimental atomic positions as well as experimental lattice parameters reported in Ref. [25] have been used for the whole interval of U_{eff} values, 0–9 eV. The differences between the relaxed and experimental structural parameters projected into the slightly different exchange coupling constants. It was found that the increase of U_{eff} values leads to the monotonous reduction of J_i parameters achieving saturation (Fig. 3). Besides that, the use of experimental structural parameters slightly enhanced the spatial anisotropy. For $U_{\text{eff}} = 6$ eV, a typical value for Cu(II)-based magnetic insulators, $R \approx 0.1$ was achieved. Both present and previous *ab initio* calculations indicate that magnetic subsystem of CUEN can be treated as a quasi-2D array of chains approximating a spatially anisotropic zigzag square lattice in Fig. 1(b).

2. *Quantum Monte Carlo calculations*

The aforedescribed first-principle calculations imply that the quantum spin-$\frac{1}{2}$ Heisenberg model on an anisotropic square lattice with a zigzag pattern [see Fig. 1(b)] represents a minimal feasible model that is needed for a deeper understanding of the spatial anisotropy in CUEN compound.

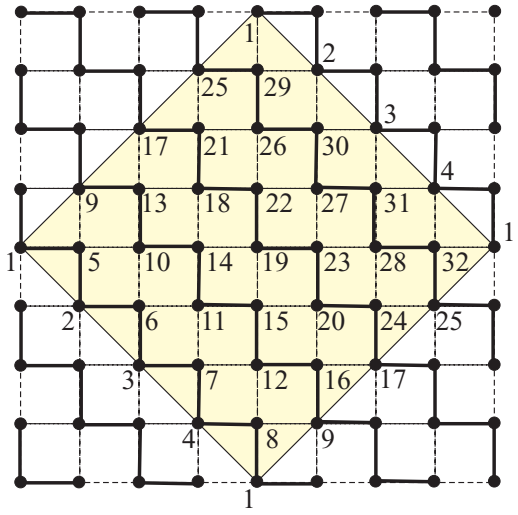

FIG. 4. An example of a finite-size lattice with the linear size $L = 4$ used for quantum Monte Carlo simulations.

Owing to this fact, let us perform a comprehensive analysis of the basic magnetic response functions (magnetization, susceptibility, and magnetic specific heat) in dependence on a relative strength of two considered coupling constants of the spin-$\frac{1}{2}$ Heisenberg model on a zigzag square lattice given by the Hamiltonian

$$H = J \sum_{\langle i,j \rangle} \boldsymbol{S}_i \cdot \boldsymbol{S}_j + J' \sum_{\langle k,l \rangle} \boldsymbol{S}_k \cdot \boldsymbol{S}_l - g\mu_B B \sum_{i=1}^{N} S_i^z. \quad (2)$$

In the above, the first summation accounts for the antiferromagnetic Heisenberg interaction ($J > 0$) between the nearest-neighbor spins from the same zigzag chain, the second summation accounts for the antiferromagnetic Heisenberg interaction ($J' > 0$) between the nearest-neighbor spins from different zigzag chains, and the last summation is the usual Zeeman's term (g is the respective Landé factor, and μ_B is Bohr magneton). The model interpolates between a HAF chain ($R = J'/J = 0$) and spatially isotropic HAF square lattice ($R = 1$).

To simulate the magnetic properties of the spin-$\frac{1}{2}$ Heisenberg zigzag square lattice, we have implemented a directed loop algorithm in the stochastic series expansion representation of the quantum Monte Carlo (QMC) method [29] from Algorithms and Libraries for Physics Simulations (ALPS) project [30]. The QMC simulations were performed on finite-size lattices (see Fig. 4) with a linear size up to $L = 128$, which involve under the periodic boundary conditions in total $N = 2L^2$ spins. This size turns up to be sufficiently large in order to avoid finite-size effects. The adequate numerical accuracy was achieved through 8×10^5 Monte Carlo steps used in addition to 2.5×10^5 steps for thermalization.

The zero-field susceptibility is plotted in Fig. 5(a) against temperature for several values of R. As one can see, the zero-field susceptibility gradually diminishes upon lowering of the spatial anisotropy (i.e., by increasing R), whereas the observed

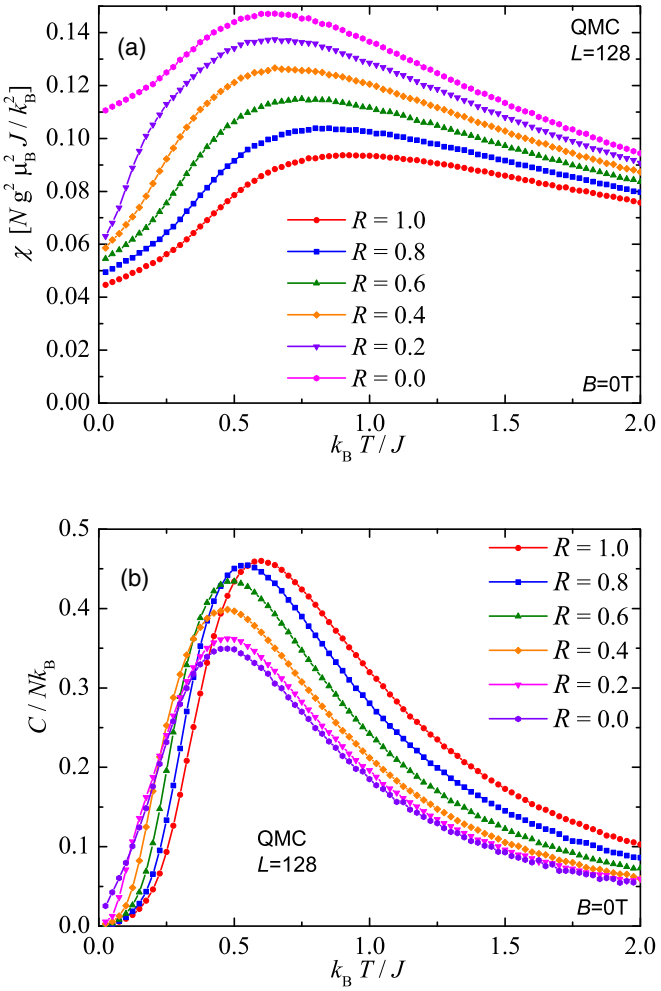

FIG. 5. Thermal variations of the zero-field susceptibility (a), and specific heat (b) of the model (2) for a few different R values.

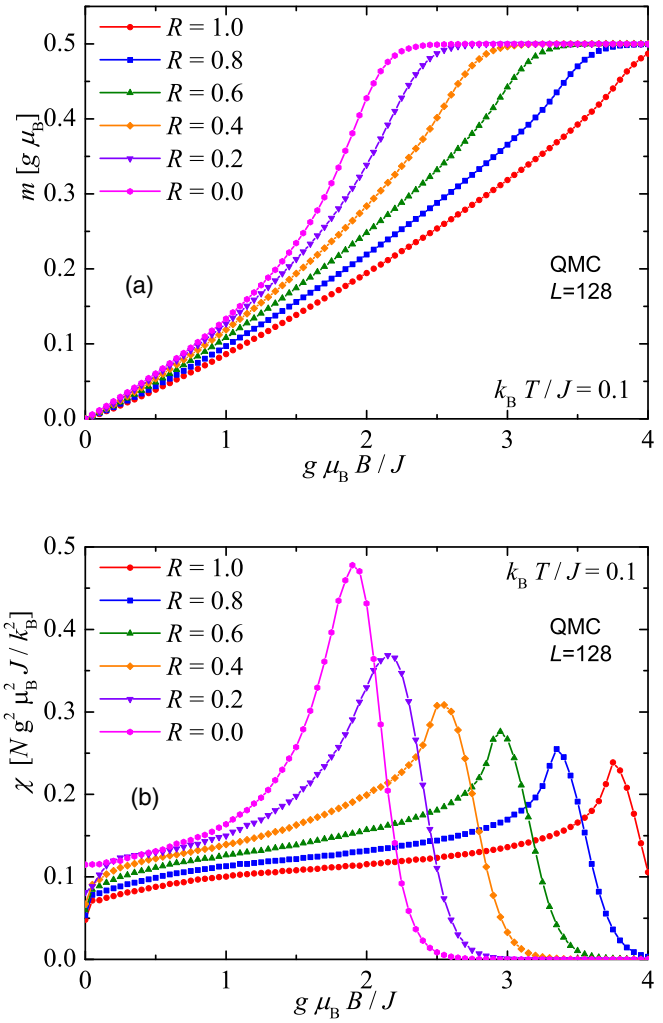

FIG. 6. The magnetization (a), and differential susceptibility (b) of the model (2) as a function of the magnetic field at the fixed temperature $k_B T/J = 0.1$, calculated for several values of R.

round maximum simultaneously shifts towards higher temperatures. For completeness, Fig. 5(b) depicts typical temperature dependencies of the zero-field specific heat for a few different values of R. It is quite evident that the specific heat shows a smooth thermal dependence with a round maximum, which height and position is in general suppressed upon strengthening of the spatial anisotropy (i.e., by lowering of the interaction ratio R). The isothermal magnetization curve is plotted in Fig. 6(a). As could be expected, the magnetization reaches the saturation value at higher magnetic fields as the interaction ratio increases. Another interesting observation is that the differential susceptibility [see Fig. 6(b)] exhibits a marked maximum slightly below a saturation field. The maximum progressively increases its height as the interaction ratio decreases.

B. Exchange anisotropy in CUEN: Symmetry constraints

Referring to the results of the first-principle calculations and previous experimental studies, only spin interactions in the basal bc plane will be considered. In the following, spin vectors are denoted by their standard symbol $\boldsymbol{S}$, or by $\boldsymbol{\mathcal{A}}, \boldsymbol{\mathcal{B}}, \boldsymbol{\mathcal{C}}, \boldsymbol{\mathcal{D}}$ when a distinction among the four sublattices becomes necessary (Fig. 2). The spin interactions in the basal and the middle bc planes are completely isomorphic due to the pure fractional translation $\tau = (\frac{1}{2}, \frac{1}{2}, 0)$ in the space group $C2/c$, which maps the interactions between $\boldsymbol{\mathcal{AB}}$ spins in the basal plane to those between $\boldsymbol{\mathcal{CD}}$ spins in the middle plane. The corresponding spin Hamiltonian can be written in the general form

$$W = \sum_{\langle kl \rangle} [J_{kl}(\boldsymbol{S}_k \cdot \boldsymbol{S}_l) + \boldsymbol{D}_{kl} \cdot (\boldsymbol{S}_k \times \boldsymbol{S}_l)] + \frac{1}{2} \sum_{\langle kl \rangle} \sum_{i,j} G_{kl}^{ij} \left(S_k^i S_l^j + S_k^j S_l^i \right) - \sum_l (g \mu_B \boldsymbol{B} \cdot \boldsymbol{S}_l), \tag{3}$$

where $\boldsymbol{S}_k$ is the spin localized at site k, which satisfies the classical constraint $\boldsymbol{S}_k^2 = s^2$. The first and the second terms in Eq. (3) describe the isotropic exchange interaction and antisymmetric Dzyaloshinskii-Moriya [31] (DM) anisotropy, respectively. The third term contains all symmetric exchange anisotropies. The interactions run over in-plane bonds denoted by $\langle kl \rangle$. The indices i and j are summed over the three values corresponding to the Cartesian components of the spin vectors

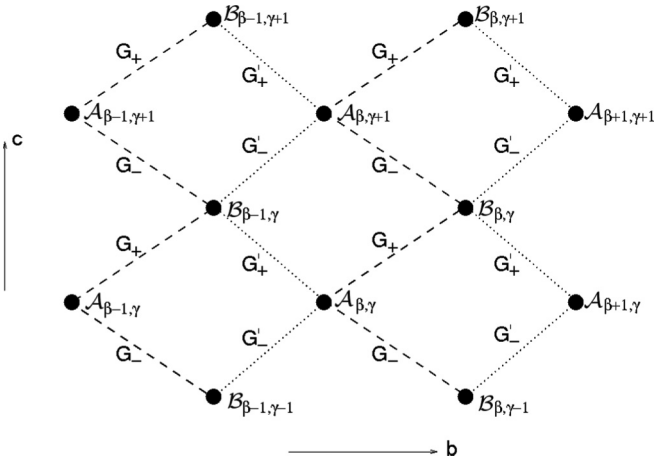

FIG. 7. Distribution of the symmetric exchange spin interaction matrices on a finite portion of the basal bc plane. The greek indices β and γ advance along the crystal axes b and c, respectively. Spin interactions in the middle bc plane are completely isomorphic, and may be obtained from this figure by the simple substitution $\mathcal{A}_{\beta,\gamma} \to \mathcal{C}_{\beta,\gamma}, \mathcal{B}_{\beta,\gamma} \to \mathcal{D}_{\beta,\gamma}$. Dashed and dotted lines represent bonds between NNN and NN Cu atoms, respectively.

along the axes a, b, and c' (Fig. 2). Finally, the last term describes the usual Zeeman interaction.

Our complete symmetry analysis is restricted to the nearest-neighbor (NN) and next-nearest-neighbor (NNN) exchange couplings. The denotation corresponds to the spatial distances between Cu atoms within the bc plane (Fig. 7). Consequently, the isotropic exchange constant J_{kl} can take two values

$$\begin{aligned} J_{kl} &= J \quad \text{for NNN in-plane neighbors, and} \\ J_{kl} &= J' \quad \text{for NN in-plane neighbors.} \end{aligned} \tag{4}$$

A nonstandard notational setting for J and J' (corresponding to J_4 and J_6 in Fig. 2) should be attributed to the fact that, according to *ab initio* calculations [22], the strongest interaction (J) occurs between the *next-nearest-neighbor* Cu atoms.

The bond centers in Fig. 7 have inversion symmetry I, which precludes the existence of the antisymmetric DM interactions ($\boldsymbol{D}_{kl} = 0$). However, the inversion symmetry does not affect any of the symmetric terms, so all elements are allowed in the symmetric anisotropic exchange tensor. The bonds G_+ and G_- (G'_+ and G'_-) are related by the c-type glide operation $\tilde{\sigma}_b = \sigma_b + (0,0,\frac{1}{2})$, where σ_b is the reflection about the plane $b = 0$. No other restrictions are imposed on the interactions matrices; all other elements of the unit-cell symmetry group can be generated from the fundamental set τ, I, $\tilde{\sigma}_b$ by suitable group multiplications.

Therefore, all symmetric exchange anisotropies are described by the four distinct matrices

$$G_+ = \begin{pmatrix} G_{aa} & G_{ab} & G_{ac'} \\ G_{ab} & G_{bb} & G_{bc'} \\ G_{ac'} & G_{bc'} & G_{c'c'} \end{pmatrix},$$

$$G_- = \begin{pmatrix} G_{aa} & -G_{ab} & G_{ac'} \\ -G_{ab} & G_{bb} & -G_{bc'} \\ G_{ac'} & -G_{bc'} & G_{c'c'} \end{pmatrix}$$

for NNN in-plane neighbors, and

$$G'_+ = \begin{pmatrix} G'_{aa} & G'_{ab} & G'_{ac'} \\ G'_{ab} & G'_{bb} & G'_{bc'} \\ G'_{ac'} & G'_{bc'} & G'_{c'c'} \end{pmatrix},$$

$$G'_- = \begin{pmatrix} G'_{aa} & -G'_{ab} & G'_{ac'} \\ -G'_{ab} & G'_{bb} & -G'_{bc'} \\ G'_{ac'} & -G'_{bc'} & G'_{c'c'} \end{pmatrix} \tag{5}$$

for NN in-plane neighbors, which are distributed as shown in Fig. 7. The above matrices may be considered as traceless because the isotropic component of the exchange interaction has already been accounted for by Eq. (4).

Considering the absence of frustration and weakness of exchange anisotropies, we can assume a ground state that is commensurate on each sublattice. Then, within the mean-field approximation, the energy per spin is given by

$$\begin{aligned} W_S = {} & \tilde{J}\boldsymbol{\mathcal{A}}\cdot\boldsymbol{\mathcal{B}} + \tilde{G}_{aa}\mathcal{A}_a\mathcal{B}_a + \tilde{G}_{bb}\mathcal{A}_b\mathcal{B}_b + \tilde{G}_{c'c'}\mathcal{A}_{c'}\mathcal{B}_{c'} \\ & + \tilde{G}_{ac'}(\mathcal{A}_a\mathcal{B}_{c'} + \mathcal{A}_{c'}\mathcal{B}_a) - \tfrac{1}{2}g\mu_B\boldsymbol{B}\cdot(\boldsymbol{\mathcal{A}}+\boldsymbol{\mathcal{B}}), \end{aligned} \tag{6}$$

where

$$\begin{aligned} &\tilde{J} = J + J', \quad \tilde{G}_{ii} = G_{ii} + G'_{ii}\ (i = a,b,c'), \\ &\tilde{G}_{ac'} = G_{ac'} + G'_{ac'}. \end{aligned} \tag{7}$$

A notable fact is that neither G_{ab} (G'_{ab}) nor $G_{bc'}$ ($G'_{bc'}$) enter Eq. (6) because their contribution averages out completely. The only remaining off-diagonal element $\tilde{G}_{ac'}$ in Eq. (6) can also be eliminated by rotating the axes a, c' by an angle ψ around the b axis, i.e., by the transformation

$$\begin{aligned} &(S_1 + iS_3) = (S_a + iS_{c'})e^{i\psi}, \quad S_2 = S_b, \\ &\tan 2\psi = \frac{2\tilde{G}_{ac'}}{\tilde{G}_{c'c'} - \tilde{G}_{aa}}. \end{aligned} \tag{8}$$

The above transformation defines the new orthogonal axes 1, 2, 3, whose advantage is that W_S acquires diagonal form

$$\begin{aligned} W_S = {} & \tilde{J}\boldsymbol{\mathcal{A}}\cdot\boldsymbol{\mathcal{B}} + (\tilde{G}_1\mathcal{A}_1\mathcal{B}_1 + \tilde{G}_2\mathcal{A}_2\mathcal{B}_2 + \tilde{G}_3\mathcal{A}_3\mathcal{B}_3) \\ & - \tfrac{1}{2}g\mu_B\boldsymbol{B}\cdot(\boldsymbol{\mathcal{A}}+\boldsymbol{\mathcal{B}}), \end{aligned} \tag{9}$$

where $\mathcal{A}_1$, $\mathcal{A}_2$, $\mathcal{A}_3$ ($\mathcal{B}_1$, $\mathcal{B}_2$, $\mathcal{B}_3$) are the components of the spin $\boldsymbol{\mathcal{A}}$ ($\boldsymbol{\mathcal{B}}$) along the axes 1, 2, 3.

However, a more transparent formulation of our results is obtained in terms of new variables, the normalized magnetization $\boldsymbol{m} = (\boldsymbol{\mathcal{A}} + \boldsymbol{\mathcal{B}})/2s$ and the normalized staggered magnetization $\boldsymbol{n} = (\boldsymbol{\mathcal{A}} - \boldsymbol{\mathcal{B}})/2s$, which satisfy the classical constraints $\boldsymbol{m}\cdot\boldsymbol{n} = 0$ and $\boldsymbol{m}^2 + \boldsymbol{n}^2 = 1$. Note that $\boldsymbol{m}$ is related to the magnetization $\boldsymbol{M}$ expressed in physical units as $\boldsymbol{M} = g\mu_B s\boldsymbol{m}$.

To ascertain the relative significance of individual terms in Eq. (9), we can employ a dimensionless scale ε [32] to introduce rescaled anisotropies $g_1 = -2\tilde{G}_1/\varepsilon^2\tilde{J}$, $g_2 = -2\tilde{G}_2/\varepsilon^2\tilde{J}$, $g_3 = -2\tilde{G}_3/\varepsilon^2\tilde{J}$ and magnetic field $\boldsymbol{h} = g\mu_B\boldsymbol{B}/2s\varepsilon\tilde{J}$.

The magnetization $\boldsymbol{m}$ is treated as a quantity of order ε, whereas the staggered magnetization $\boldsymbol{n}$ and the rescaled variables are assumed to be of order of unity. Then, to leading order, the classical constraints reduce to $\boldsymbol{m}\cdot\boldsymbol{n} = 0$ and $\boldsymbol{n}^2 = 1$. Finally, the (rescaled) energy per spin, measured

in units $\tilde{J}\varepsilon^2 s^2$, is expressed entirely in terms of the staggered magnetization $\boldsymbol{n}$,

$$w_S = \tfrac{1}{2}\left[g_1 n_1^2 + g_2 n_2^2 + g_3 n_3^2\right] + \tfrac{1}{2}(\boldsymbol{n}\cdot\boldsymbol{h})^2, \qquad (10)$$

and n_1, n_2, n_3 are the components of $\boldsymbol{n}$ taken along the axes 1, 2, 3. We note that the energy of the pure Néel state has already been removed from the above expression. The magnetization $\boldsymbol{m}$ is also expressed in terms of $\boldsymbol{n}$:

$$\boldsymbol{m} = -\frac{\varepsilon}{2}[\boldsymbol{n}\times(\boldsymbol{n}\times\boldsymbol{h})]. \qquad (11)$$

Although Eq. (9) is more general than Eq. (10), the latter provides adequately accurate results as long as all anisotropies $\tilde{G}_1, \tilde{G}_2, \tilde{G}_3$ and the applied field $g\mu_B B/s$ are sufficiently weak compared to the exchange constant $\tilde{J}$.

In the absence of external fields ($\boldsymbol{h} = 0$), w_s in Eq. (10) is minimized by the Néel state polarized along the easy axis, determined by $\min\{g_1, g_2, g_3\}$. The net magnetization, given by Eq. (11), is zero. For a field applied along the easy axis, the antiferromagnetic (AF) ground state first remains spin polarized along the same axis with $\boldsymbol{m} = 0$. A spin-flop (SF) transition occurs at the critical field $h_{\rm SF}$ above which minimum energy is achieved for the configuration with $\boldsymbol{n}$ perpendicular to the easy axis; the actual direction of $\boldsymbol{n}$ is determined by $\min\{\{g_1, g_2, g_3\}\backslash\min\{g_1, g_2, g_3\}\}$, where $\backslash$ denotes set complement. The transition is accompanied by a sudden jump in the magnetization along the direction of the applied field, which further grows linearly with h as dictated by Eq. (11). We mention that the dimensionless anisotropy constant along the easy axis in Eq. (10) can be set equal to zero without any loss of generality. The remaining two anisotropies can be taken positive, the smaller of the two would equal to $h_{\rm SF}^2$. However, in view of uncertainty regarding the actual direction of the easy axis, we keep Eq. (10) for the moment in its current form.

IV. EXPERIMENTAL RESULTS AND DISCUSSION

A. Exchange anisotropy in CUEN

1. *Magnetic susceptibility*

Temperature dependence of magnetic susceptibility χ was studied at temperatures from 0.5 to 8 K. The measurements were performed in the field-cooling (FC) and zero-field-cooling (ZFC) regimes. The magnetic field $B = 10$ mT was applied along the a, b, and c' directions (Fig. 8).

The data are characterized by a round maximum at about 2.5 K resulting from the contribution of short-range magnetic correlations. The transition to the long-range magnetic order manifests as a sharp minimum appearing at about 0.93 K in all studied directions (Figs. 8 and 9). All FC and ZFC data coincide in the paramagnetic phase. In the ordered phase, FC and ZFC data bifurcate for the fields applied along the a and c' directions, while they remain identical for $B \parallel b$. The observed spatial anisotropy in χ clearly reflects the anisotropy of g factor, as already indicated by EPR and susceptibility studies, $g_a > g_{b,c'}$ and $g_b \sim g_{c'}$ [24]. To exclude the effects introduced by g factors, susceptibility data were normalized properly, considering conclusions of previous Monte Carlo calculations [13].

The MC studies investigated the effects of extremely weak exchange anisotropies on the finite-temperature properties of

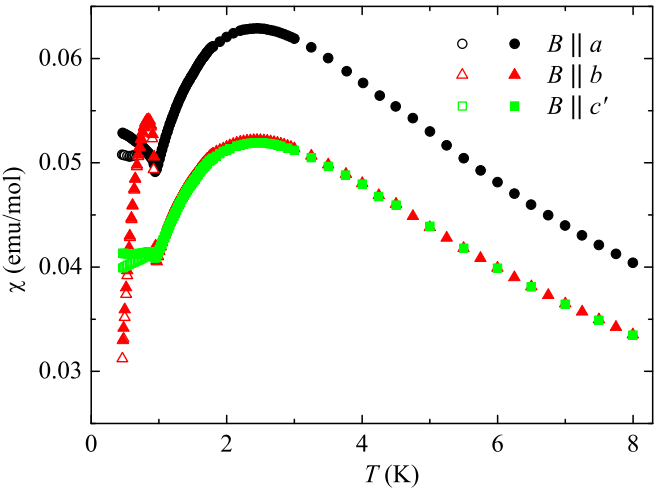

FIG. 8. Temperature dependence of CUEN susceptibility in the field 10 mT applied along the a, b, and c' directions. Full and open circles correspond to data obtained in FC and ZFC regimes, respectively.

a spin-$\frac{1}{2}$ XXZ model on the square lattice ($R = 1$) described by the Hamiltonian [13]

$$H = J\left[\sum_{i,d}(1-\Delta_\mu)\left(S_i^x S_{i+d}^x + S_i^y S_{i+d}^y\right) + (1-\Delta_\lambda)S_i^z S_{i+d}^z\right]. \qquad (12)$$

The parameter $i = (i_1, i_2)$ runs over all sites of the square lattice and d connects each site to its four nearest neighbors. Aside from isotropic HAF model ($\Delta_{\lambda,\mu} = 0$), Eq. (12) defines a system with easy-axis ($\Delta_\lambda = 0$, $0 < \Delta_\mu \leqslant 1$) or easy-plane exchange anisotropy ($\Delta_\mu = 0$, $0 < \Delta_\lambda \leqslant 1$). The study revealed that for extremely weak exchange anisotropies $\Delta_{\lambda,\mu} \approx 10^{-2}$, the uniform susceptibility follows the prediction for the isotropic model at sufficiently high temperatures comparable to J while at about $0.3J$, a crossover to the anisotropic easy-axis or easy-plane (XY) regime appears.

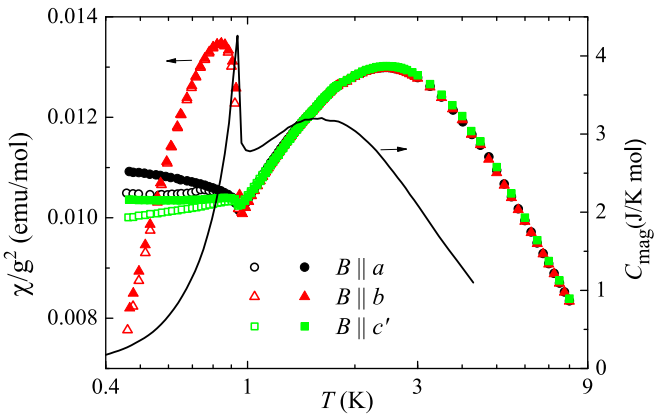

FIG. 9. Temperature dependence of normalized CUEN susceptibility in the field 10 mT. Full and open symbols represent data obtained in FC and ZFC regimes, respectively. The solid line represents the magnetic specific heat of CUEN in $B = 0$ T.

Hence, CUEN susceptibility data were normalized at temperatures above 2 K ($\approx 0.7 J_{\rm eff}$) to obtain a universal curve χ/g^2. The g values

$$g_a = 2.200, \quad g_b = 2.005, \quad \text{and } g_{c'} = 2.000, \qquad (13)$$

used in the normalization, within the experimental accuracy correspond to those extracted from the susceptibility analysis in Ref. [24]. The normalization was extrapolated down to the lowest temperatures (Fig. 9).

As can be seen, in the paramagnetic phase, only slight deviations from the universal curve appear in the vicinity of a phase transition as a result of extreme weakness of the exchange anisotropy. In such a case, a reliable indication of the aforementioned 2D Heisenberg-Ising or XY crossover is not possible. On the other hand, a significant anisotropy of χ/g^2 persisting in the ordered phase can be ascribed to the effect of the exchange anisotropies. The low-temperature susceptibility data (Fig. 9) show that CUEN is not a simple XXZ system described by Eq. (12). Considering the results of the symmetry analysis in Sec. III B, two exchange anisotropies can be expected in CUEN; an easy-plane (out-of-plane) anisotropy Δ_λ [in coincidence with a notation in Eq. (12)], and in-plane exchange anisotropy $\Delta_{\rm in}$. The latter is associated with the presence of the symmetry-breaking easy axis within the easy plane and $\Delta_\lambda > \Delta_{\rm in}$.

At this moment, there are no theoretical predictions for the uniform susceptibility of the XYZ model on the square lattice, so we can believe that the extraordinary behavior of CUEN susceptibility observed along the b axis, namely, the absence of FC-ZFC difference and a steep decrease of the susceptibility below the second maximum appearing around 0.85 K, support a conjecture about identifying the b axis as the easy axis of the system. It should be noted that previous studies [24] revealed the presence of DM anisotropy in the interlayer coupling. This mechanism could be considered as a possible source of hidden spin canting which might lead to the observed behavior of the susceptibility along the b axis.

2. *Magnetization*

Magnetic-field dependence of magnetization was studied at constant temperatures below a phase transition ($T = 0.5$ and 0.8 K) and above the phase transition (1.2 K) in magnetic fields applied along the a, b, and c' directions (Fig. 10). Despite relatively large temperature interval ranging from about 0.5 T_N to 1.3 T_N, thermal fluctuations do not seem to play a significant role. A tiny increase of magnetization at 1.2 K indicates that thermal fluctuations slightly enhance polarizing effects of external magnetic field. The individual components of a magnetic moment induced in the field 5 T achieve values $\approx 0.5\mu_B$, which represents only half of the full moment per Cu(II) ion. It reflects rather strong influence of intralayer antiferromagnetic correlations with 2D saturation field, $B_{\rm sat}^{\rm 2D}$, higher than 5 T. Previous powder studies [21] estimated $B_{\rm sat}^{\rm 2D} = 7.2$ T.

In the low-field region below 0.5 T, magnetization curve is linear in the field applied along the a and c' directions at all studied temperatures. In the field parallel to the b axis, the linearity is observed only in the data taken above T_N, while below T_N an anomalous jump appears in the field ≈ 200 mT (Fig. 10, upper insets). As mentioned in Sec. III B, a spin-flop transition should be expected in the field applied along the easy axis.

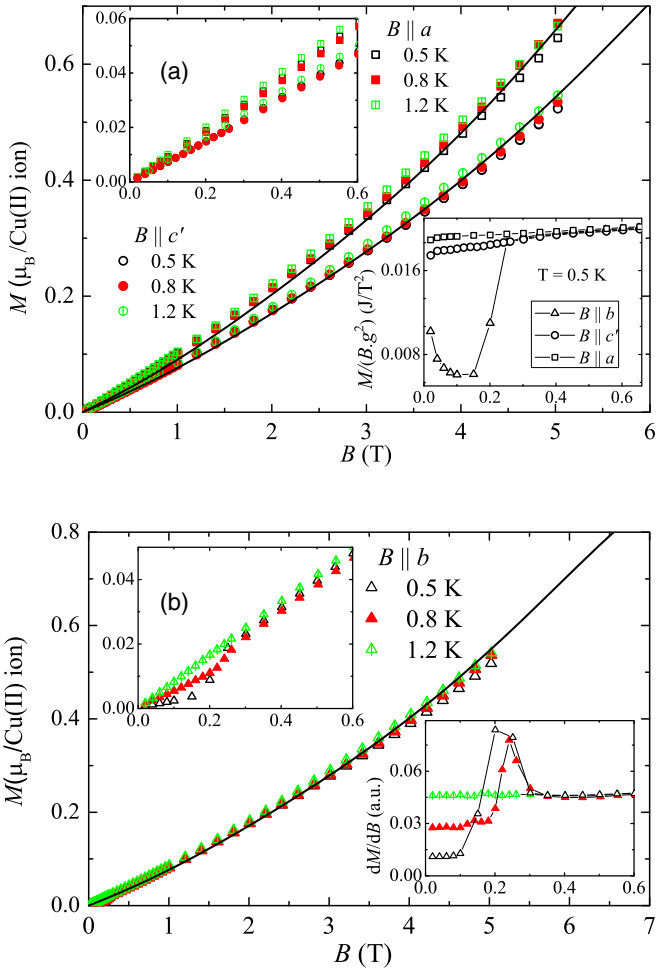

FIG. 10. Isothermal magnetization of CUEN studied in the field applied along the a, b, and c' directions. Solid lines represent QMC calculations of magnetization ($L = 128$) for the model (2) with $J/k_B = 3.6$ K, $R = 0.35$, and $T = 0.8$ K. The g factors were taken according to Eq. (13). Upper insets: zooming of the low-field region. Lower insets: (a) $M/(Bg^2)$ in the low-field region at 0.5 K (see text). (b) Derivative of magnetization in the low-field region $B \parallel b$.

Therefore, the b axis (or axis 2 from Sec. III B) can be identified with the easy axis. By further noting that the angle ψ from the transformation in Eq. (8) is defined up to the integer multiple of $\pi/2$, we can deliberately assume that $\tilde{G}_2 > \tilde{G}_3 > \tilde{G}_1$. Then, the anisotropies in Eq. (9) can be rewritten in the form of the in-plane exchange anisotropy $\tilde{G}_{\rm in} \equiv (\tilde{G}_2 - \tilde{G}_3)$, and out-of-plane exchange anisotropy $\tilde{G}_{\rm out} \equiv (\tilde{G}_2 - \tilde{G}_1)$, and $\tilde{G}_{\rm out} > \tilde{G}_{\rm in}$. They correspond to aforementioned Δ_λ and $\Delta_{\rm in}$ through the relation

$$\Delta_\lambda = \frac{\tilde{G}_{\rm out}}{\tilde{J}}, \quad \Delta_{\rm in} = \frac{\tilde{G}_{\rm in}}{\tilde{J}}. \qquad (14)$$

Similarly, $g_{\rm in} \equiv (g_3 - g_2)$, $g_{\rm out} \equiv (g_1 - g_2)$, and $g_{\rm out} > g_{\rm in} > 0$. Then, Eq. (10) can be rewritten as

$$w_S = (1/2)\big[g_{\rm out} n_1^2 + g_{\rm in} n_3^2 + (\boldsymbol{n} \cdot \boldsymbol{h})^2\big], \qquad (15)$$

where the irrelevant constant term was omitted.

In the absence of the external field, the ground state is achieved by the configuration $n_2 = \pm 1$, $n_1 = n_3 = 0$, and $\boldsymbol{m} = 0$. When the field is applied along the easy axis, the above configuration with the energy $w_s = h^2/2$ remains stable until $h^2 < h_{\rm SF}^2 = g_{\rm in}$. For higher fields, $h > h_{\rm SF}$, the energy is minimized by the configuration $n_3 = \pm 1$, $n_1 = n_2 = 0$, i.e., spins flip within the easy plane from the easy axis 2 to the middle axis 3 and the ground state develops a nonzero net magnetization along the easy axis $m_2 = h\varepsilon/2$ as dictated by Eq. (11). In physical units,

$$(g_b \mu_B B_{\rm SF})^2 = 8\tilde{J} s^2 \tilde{G}_{\rm in}. \tag{16}$$

To obtain a more accurate experimental estimate of the spin-flop field, a derivative of the magnetization dM/dB was calculated [Fig. 10(b), lower inset]. Then, the position of the maximum was taken as the critical field [33], namely, 220 ± 20 mT and 250 ± 10 mT for dM/dB at 0.5 and 0.8 K, respectively. Considering the critical field at 0.5 K as the estimation of the spin-flop field, the application of Eqs. (14) and (16) with $g_b = 2.005$, $s = \frac{1}{2}$ and the effective intralayer coupling $\tilde{J}/k_B \equiv 2J_{\rm eff}/k_B = 5.6$ K, provides the estimate $\Delta_{\rm in} \approx 1.4 \times 10^{-3}$. The value is within the range of exchange anisotropies observed in quasi-2D Cu(II)-based antiferromagnets [33,34].

The exchange anisotropies (14) introduce $k = 0$ gaps in the magnon spectrum. In the absence of magnetic fields,

$$\hbar\Omega_{\rm in} = 2s\sqrt{2\tilde{J}\tilde{G}_{\rm in}},\ \hbar\Omega_{\rm out} = 2s\sqrt{2\tilde{J}\tilde{G}_{\rm out}}. \tag{17}$$

Note that the lower magnon gap (in the absence of magnetic fields) can be expressed as

$$\hbar\Omega_{\rm in} = g_b \mu_B B_{\rm SF}, \tag{18}$$

and depends only on the measured value of $B_{\rm SF}$. Using $g_b = 2.005$ and $B_{\rm SF} = 0.22$ T, the predicted lower magnon gap is about 0.3 K. It would be interesting to verify this prediction in the antiferromagnetic resonance experiment.

Both anisotropies affect the development of a ground-state ($T = 0$) magnetization, obtained by a direct minimization of Eq. (9):

$$M_1 = \frac{g_1^2 \mu_B^2 B}{4[\tilde{J} + 1/3(\tilde{G}_{\rm out} + \tilde{G}_{\rm in})] - 2\tilde{G}_{\rm out}}, \quad B \parallel 1$$

$$M_3 = \frac{g_3^2 \mu_B^2 B}{4[\tilde{J} + 1/3(\tilde{G}_{\rm out} + \tilde{G}_{\rm in})] - 2\tilde{G}_{\rm in}}, \quad B \parallel 3$$

and finally for $B \parallel 2$

$$M_2 = \begin{cases} 0, & B < B_{\rm SF} \\ \frac{g_b^2 \mu_B^2 B}{4[\tilde{J} + 1/3(\tilde{G}_{\rm out} + \tilde{G}_{\rm in})] - 2\tilde{G}_{\rm in}}, & B > B_{\rm SF}. \end{cases} \tag{19}$$

It is clear that a reduced magnetization $M_i/(B_i g_i^2)$ along the hard axis ($i = 1$) is predicted to grow faster than magnetizations for the fields applied in the 23 plane. Moreover, above the spin-flop transition, both reduced magnetizations ($i = 2,3$) should grow with the same rate.

Using aforementioned g factors (13), reduced experimental magnetizations were calculated for a, b, c' at the lowest temperature $T = 0.5$ K [Fig. 10(a), lower inset]. A qualitative comparison of the experimental data with the prediction (19) suggests that at least within a few degrees, the axes 1 and 3 could coincide with the a and c' directions, respectively. The identification of the hard axis can be supported by previous EPR studies which revealed the presence of the exchange anisotropy, with the easy plane bc^*, perpendicular to the a axis [24]. The coincidence of the easy plane bc^* with the equatorial plane of a local octahedron significantly elongated along the a axis (Fig. 2) suggests that a weak single-ion anisotropy produced within the octahedron [35] might contribute to the observed effective exchange anisotropy in CUEN. Recall that the axis 2 coincides with the crystallographic b axis by definition. This choice of the anisotropy axes corresponds to extremal values of g factors observed in previous EPR studies [24]. Thus, the intrinsic spin anisotropy in CUEN can result from the interplay of dipolar coupling between Cu(II) ions [24], single-ion anisotropy within the CuO_4N_2 units [35], and virtual hopping of electrons between ground and excited orbitals of neighboring Cu(II) ions [36]. Additional *ab initio* studies that include spin-orbit interaction are required to further clarify the role of individual contributions.

It should be noted that within the experimental accuracy, in higher fields above ≈0.5 T, the differences between the reduced data completely vanish and they fall on a universal curve. Such behavior could be ascribed to the prevailing effect of magnetic field after compensating the influence of weak exchange anisotropies. Potentially, in higher fields, the system might mimic an isotropic Heisenberg in external magnetic field. Consequently, a field-induced Berezinskii-Kosterlitz-Thouless transition could be observed as predicted in Ref. [14].

B. Spatially anisotropic square lattice in CUEN

As was shown in Sec. III A 1, a spatial distribution of exchange interactions in CUEN approximates a spatially anisotropic zigzag square lattice with $R \approx 0.15$. A model of Heisenberg antiferromagnet ($\Delta_{\lambda,\mu} = 0$) on the corresponding lattice studied in Sec. III A 2 was applied in the analysis of a normalized experimental susceptibility above a phase transition [Fig. 11(a)]. The best agreement with experimental data was achieved for the intrachain coupling $J/k_B \approx 3.7$ K and $R \approx 0.35$. Concerning experimental magnetization data which are nearly insensitive to temperature (Fig. 10), QMC calculations were performed at 0.8 K and a reasonable agreement was achieved for $J/k_B = 3.6$ K and $R = 0.35$. Very similar fitting set of the interaction parameters was also obtained from the analysis of the specific-heat data in zero magnetic field, namely, $J/k_B \approx 3.4$ K and $R \approx 0.35$ [Fig. 11(b)]. A difference between the R extracted from the present analysis and the *ab initio* calculations could be ascribed to a combined influence of spin-orbit coupling and hydrogen bonds present in the structure of CUEN. The improvement could be achieved by incorporation of spin-orbit coupling and van der Waals interactions, which could modify the *ab initio results* by accounting for the influence of H-O and N-H bridges [37].

Considering deviations from 2D behavior, previous quantum MC studies [39] of HAF square lattice ($R = 1$) with interlayer coupling J'' provided the estimation of the ordering temperature as a function of J''. While for isotropic HAF on a simple cubic lattice ($\Delta_{\lambda,\mu} = 0$, $J''/J \approx 1$) the ordering temperature is $k_B T_N/J \approx 0.95$, in CUEN the corresponding

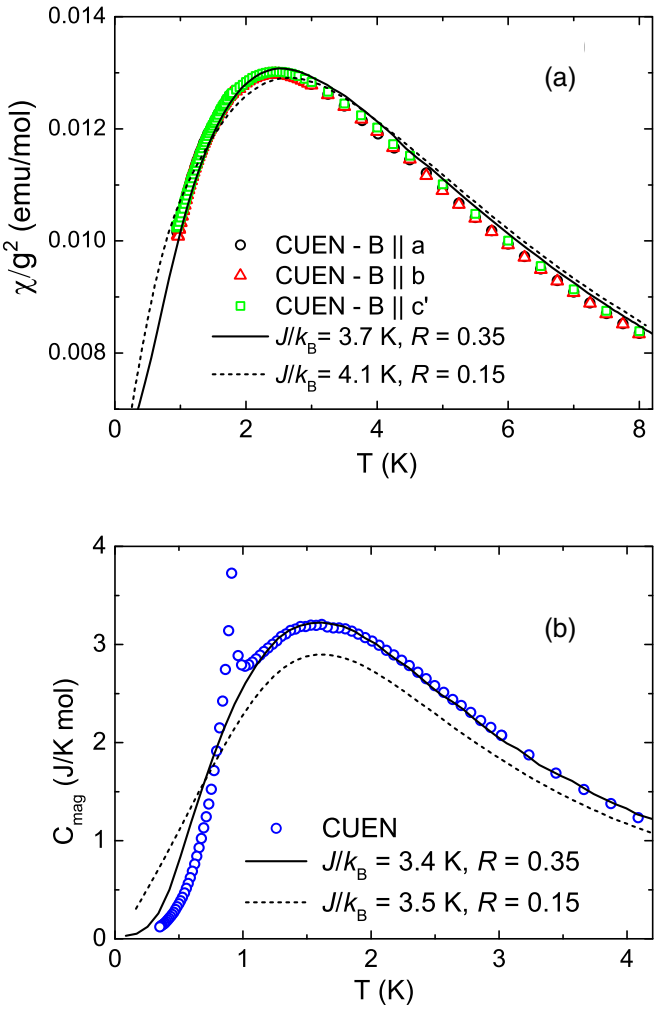

FIG. 11. (a) Temperature dependence of normalized CUEN susceptibility in the field 10 mT. Open symbols represent data in ZFC regime. Solid and dashed lines represent corresponding QMC calculations ($L = 128$) for the model (2) with $R = 0.35$ and 0.15, respectively. (b) Temperature dependence of magnetic specific heat of CUEN single crystal in zero magnetic field. A lattice contribution in the effective form of $0.003T^{2.8}$ has been subtracted from the total specific heat [38]. Solid and dashed lines represent corresponding QMC calculations ($L = 128$) of the specific heat for the model (2) with $R = 0.35$ and 0.15, respectively.

ratio $k_B T_N/J_{\rm eff}$ is reduced to the value $\approx$0.3, indicating a strong 2D character of magnetic correlations with $J''/J_{\rm eff} \lesssim 0.03$. To include the effect of the intralayer spatial anisotropy, alternative approach was applied to estimate the strength of J'' by using a relation [40]

$$k_B T_N = J''\left(\frac{N}{N_0}\right)^2\left(\frac{\xi}{a}\right)^2. \qquad (20)$$

Parameter a represents a lattice constant, and N/N_0 is the reduction in the $T = 0$ staggered magnetization relative to the Néel value induced by 2D quantum fluctuations at length scales shorter than the intralayer correlation length ξ. MC studies [7,9] of a spatially anisotropic square lattice [Fig. 1(a)] provided for $R = 0.3$ a reduced value of the staggered magnetization $N \sim 0.25$, as well as a reduction of correlation lengths $\xi_{\rm chain}/a \approx 6$ and $\xi_{\rm interchain}/a \approx 2$. Both values are lower than previously estimated $\xi/a \approx 14$ for the isotropic square lattice at the transition temperature in CUEN [21]. For $T_N = 0.93$ K and aforementioned intrachain correlation length, Eq. (20) provides the estimation of the interlayer coupling $J''/k_B \approx 0.1$ K, which agrees very well with the aforementioned estimate $J''/J_{\rm eff} \lesssim 0.03$.

For such a low ratio, the MC studies [39] predict much lower height of the specific-heat peak. The difference can be ascribed not only to finite-size effects accompanying MC calculations, but also to the presence of the easy-axis exchange anisotropy in CUEN. The latter together with a nonzero J'' support the ordering process at T_N.

The aforementioned estimate of the spatial anisotropy of the intralayer exchange coupling allowed to refine the strength of the in-plane exchange anisotropy. Taking $\tilde{J} = J(1 + R)$ then the values $J/k_B = 3.4$ K and $R = 0.35$ provide $\tilde{J}/k_B \cong 4.6$ K, and application of Eqs. (14) and (16) yields $\Delta_{\rm in} \approx 2 \times 10^{-3}$. This value is about one order of magnitude lower than the ratio $J''/J_{\rm eff}$, suggesting the predominance of the interlayer coupling in the ordering process in CUEN. The prevalence of the interlayer correlations might also manifest in the coincidence of the transition temperature with the position of a minimum appearing in the susceptibilities along the b and c' directions (Fig. 9).

C. Magnetic phase diagrams of CUEN

Previous studies [23] of a magnetic B-T phase diagram of CUEN in the magnetic field applied along the a axis revealed the enhancement of transition temperatures which is a typical feature of a field-induced Berezinskii-Kosterlitz-Thouless (BKT) phase transition [14]. Quantum MC calculations [17] showed that this characteristic preserves in highly anisotropic quasi-2D magnets, i.e., the systems with extremely weak interlayer coupling. The applied magnetic field reduces the amplitude of phase fluctuations and the magnitude of the order parameter [17]. The former dominates in a low-field regime and increases the entropy $S^{\rm 3D}$ and the amplitude of the specific-heat anomaly $C^{\rm 3D}$ associated with a 3D ordering process. The diminishing of the order parameter in higher magnetic fields is accompanied with the decrease of a transition temperature as well as both $S^{\rm 3D}$ and $C^{\rm 3D}$ quantities [17].

Such a behavior of the entropy and the specific-heat anomaly was already observed in CUEN in the field applied along the a axis [23]. Thus, for completeness, we investigated B-T diagrams in the fields applied along the b and c' directions. A temperature dependence of specific heat was measured in constant magnetic fields (Fig. 12). It is obvious that in both directions, an enhancement of a transition temperature and $C^{\rm 3D}$ occurs in the fields up to about 2 T. A slight anisotropy of B-T diagrams (Fig. 13) is fully determined by the g-factor anisotropy, as manifested by the behavior of the Bg product. Within experimental accuracy, the data fall on a nearly universal curve for all three orientations (Fig. 13, inset). It can be seen that the shape of the phase diagrams mimics the BKT transition expected for the isotropic Heisenberg square lattice in applied magnetic fields [14]. However, theoretical saturation fields are rather overestimated as a result of existing

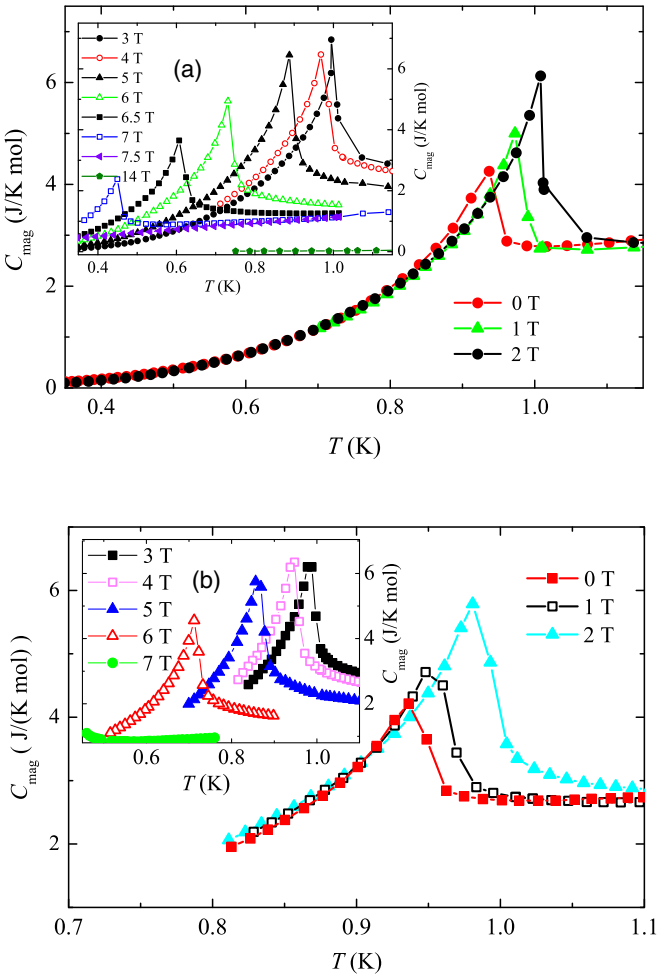

FIG. 12. Temperature dependence of magnetic specific heat of CUEN single crystal in a magnetic field (a) $B \parallel b$, (b) $B \parallel c'$. For clarity, only data for selected field values are depicted.

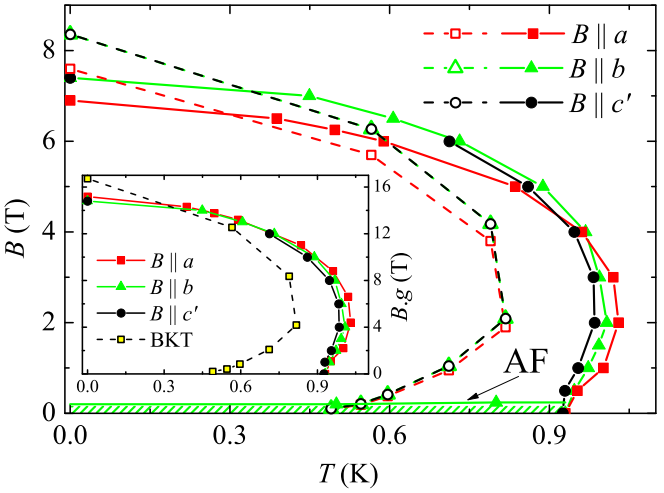

FIG. 13. B-T phase diagram of CUEN single crystal as derived from specific-heat data (full symbols). For $B \parallel b$, also the AF phase derived from the isothermal magnetization is depicted. The data for $B \parallel a$ are taken from Ref. [23]. Saturation fields estimated from the specific heat in 14 T are also included (see text). Open symbols represent the theoretical predictions [14] for a field-induced BKT transition in HAF square lattice [$R = 1$, $J/k_B \equiv J_{\rm eff}/k_B = 2.8$ K, g factors are taken from Eq. (13)]. Inset: the same diagram, B is replaced by a product gB.

spatial anisotropy of exchange coupling within a magnetic layer in CUEN.

1. B-T diagram in B ∥ b

As was shown in Secs. III B and IV A, the symmetry of the crystal structure of CUEN supports a weak exchange anisotropy within the magnetic layer, which should influence the magnetic phase diagram at least in the region of low magnetic fields. Considering AF-SF transition within the easy plane, the B-T diagram in $B \parallel b$ was completed showing nearly negligible ordered AF phase (Fig. 13) which could not be directly identified by aforementioned specific-heat data depicted in Fig. 12.

Since the in-plane anisotropy $\Delta_{\rm in}$ is weaker than the out-of-plane anisotropy Δ_λ, in fields slightly above $B_{\rm SF}$, the spins should lie within the easy plane as in the case of the easy-plane magnet ($\Delta_{\rm in} = 0$). As was suggested in Refs. [41,42], magnetic field applied within the easy XY plane acts as an effective easy-axis exchange anisotropy breaking the XY symmetry. As a result, further increase of magnetic field leads to establishing Ising-type symmetry and the formation of 2D long-range Ising order [41,42]. It should be noted that the statement holds for a pure 2D XY magnet, i.e., $\Delta_{\rm in} = 0$, $\Delta_\mu = 0$, and $\Delta_\lambda = 1$ in Eq. (12). Experimental studies of quasi-2D magnets with extremely weak easy-plane anisotropy $\Delta_\lambda = 0.007$ suggest a field-induced Ising-type behavior only in low magnetic fields applied within the easy plane [42]. The authors believe that in higher fields a field-induced XY anisotropy develops similarly like in the case of the isotropic Heisenberg lattice [14]. This conjecture coincides with the aforementioned behavior of isothermal magnetization curves at 0.5 K falling on a universal curve above ≈0.5 T [lower inset of Fig. 10(a)]. The corresponding prediction for the saturation field of the isotropic antiferromagnet [43]

$$B_{\rm sat}^{\rm 2D} = \frac{2zJs}{g\mu_B}, \tag{21}$$

with $z = 4$, $s = \frac{1}{2}$, and $J = J_{\rm eff}$, provides $B_{\rm sat}^{{\rm 2D},b} \approx 8.3$ T, which is much higher than the previous powder estimate [21]. The inclusion of the spatial intralayer anisotropy $zJ \to 2(J + J')$ with $R = 0.35$ and $J/k_B = 3.4$ K, estimated from the specific-heat analysis, yields $B_{\rm sat}^{{\rm 2D},b} \approx 6.9$ T. The value is even lower than a critical field $B_c = 7$ T corresponding to the position of a specific-heat anomaly at $T_c = 0.45$ K in Fig. 12 and can be treated as a lower limit of a saturation field, involving only 2D correlations. Actual value should involve also the contribution of the interlayer coupling $B_{\rm sat} = B_{\rm sat}^{\rm 2D} + 2z''J''s/(g\mu_B)$ [17].

To obtain a more realistic estimate, the specific-heat data in 14 T were analyzed within a spin-wave theory [44]. Above saturation fields, a gap Δ_H opens in the spin excitation spectrum, developing linearly with magnetic field

$$\Delta_H = g\mu_B(B - B_{\rm sat}). \tag{22}$$

The corresponding specific heat is characterized by exponential behavior at sufficiently low temperatures $T < \Delta_H/k_B$:

$$C \approx \frac{\exp\left(\frac{\Delta_H}{k_B T}\right)}{T}. \quad (23)$$

Fitting the specific-heat data with Eq. (23) below 3 K, and subsequent application of Eq. (22), yields $\Delta_H/k_B = 8.9 \pm 0.3$ K and $B^b_{\rm sat} = 7.3 \pm 0.3$ T. It is clear that the experimental uncertainty ≈0.6 T is comparable with the hypothetical contribution of interlayer correlations. Considering the aforementioned value $J''/k_B \approx 0.1$ K, the field 0.6 T corresponds to $z'' \sim 8$, i.e., eight neighbors in adjacent magnetic layers. This result coincides well with the spatial distribution of Cu atoms. Specifically, each Cu atom in the bc layer has four nearest neighbors in the adjacent bc layer at distances ranging from 5.2 to 6.8 Å. Other neighbors in adjacent layers lie at distances 11 Å and more.

It should be noted that the application of Eq. (21) for J and J' obtained from the susceptibility and magnetization data analysis provides 2D saturation fields 7.45 and 7.25 T, respectively. Thus, even negligible dispersion of exchange parameters precludes reliable estimation of the contribution of 3D correlations to the saturation field.

2. *B-T diagram in B ∥ a,c′*

For the field applied along the c' direction, no spin-flop transition is expected. The spins lie in the easy plane, already perpendicular to the magnetic field. Applying the results of Ref. [41], we can speculate that for small fields up to about $B_{\rm SF}$, the same scenario with 2D Ising order can realize. For higher field, prevailing the energy of intrinsic easy-plane anisotropy Δ_λ, a field-induced XY anisotropy develops as in the case of the isotropic Heisenberg lattice [14]. The application of Eq. (21) provides the same saturation field along the c' direction as that for the field along the b axis, namely, $B^{2D,c'}_{\rm sat} \approx B^{2D,b}_{\rm sat}$.

Concerning the field applied along the a axis, i.e., perpendicular to the easy plane, theoretical studies of the square lattice with weak easy-plane exchange anisotropy Δ_λ show that at least moderate magnetic fields reinforce the planar character of the system [41,45]. A ground state becomes fully aligned at a saturation field [45]

$$B^{2D}_{\rm sat} = \frac{(2-\Delta_\lambda) z J s}{g\mu_B}. \quad (24)$$

Application of the same procedure with the specific-heat data in the field 14 T applied along the a axis yields a gap $\Delta_H/k_B = 10.9 \pm 0.3$ K and $B^a_{\rm sat} = 6.6 \pm 0.2$ T, for $g = 2.2$. On the other hand, the application of Eq. (24) with $\Delta_\lambda \approx \Delta_{\rm in}$, $R = 0.35$, $J/k_B = 3.4$ and 3.7 K provides the saturation fields $B^{2D,a}_{\rm sat} = 6.2$ and 6.8 T, respectively.

It is obvious that in CUEN, unlike the spatial anisotropy of intralayer exchange coupling, the exchange anisotropy has a negligible effect on the saturation fields. However, the extremely weak exchange anisotropy and relatively strong 2D quantum fluctuations seem to play an important role in the determination of the symmetry of the order parameter. Preliminary study [46] of the temperature dependence of a magnetic Bragg reflection (001) in zero magnetic field revealed a critical index $\beta = 0.18$, which is very close to 0.125, a value predicted for a 2D Ising universality class.

V. CONCLUSION

First-principle calculations of exchange interactions in CUEN confirmed that the system represents a 2D array of coupled chains forming a zigzag square lattice within the bc layer. Using quantum Monte Carlo calculations, finite-temperature properties including specific heat, magnetization, and uniform susceptibility were calculated for the zigzag square lattice with various strength of a spatial anisotropy ranging from independent chains ($R = 0$) to a square lattice ($R = 1$). The analysis of experimental single-crystal magnetic susceptibility, specific heat, and magnetization confirmed the presence of a spatial anisotropy of exchange couplings within a magnetic layer as expected from first-principle calculations.

Theoretical analysis of the underlying crystal symmetry in CUEN restricted to NN and NNN spin interactions within the bc layer ruled out the presence of Dzyaloshinskii-Moriya interactions. The symmetric exchange anisotropies were described within a concept of out-of-plane and in-plane exchange anisotropies. Consequent analysis of experimental data enabled the identification of the easy plane with the bc' plane and the in-plane easy axis with the b axis.

Magnetic phase diagrams studied in a wide range of magnetic fields show only weak dependence on the field orientation. The main feature is a nonmonotonous development of transition temperatures characteristic for a field-induced Berezinskii-Kosterlitz-Thouless phase transition [14]. Another feature, a spin flop within the easy plane in the field applied along the b axis, arises from the interplay of the magnetic field and the weak exchange anisotropy. In the other two orientations a and c', only one phase was detected.

It is obvious that the application of magnetic field can change the universality class of a phase transition in quasi-2D magnets, depending on the orientation of magnetic field. Up to now, theoretical studies of a square lattice with a weak easy-plane exchange anisotropy Δ_λ in the field applied within the easy plane are missing. For a 2D XY model on the square lattice, existing theoretical studies unambiguously indicate a field-induced 2D Ising behavior [41]. It is not clear whether this result can be directly extrapolated also for the case of rather weak exchange anisotropies ($\Delta_\lambda \approx 10^{-3}$–$10^{-2}$) typical for real quasi-2D magnets. Experimental studies [42] suggest that in such systems, a crossover between low-field-induced 2D Ising behavior and higher-field-induced XY regime exists. A more complicated situation can be expected in the low-field region of magnets with nonzero in-plane exchange anisotropy $\Delta_{\rm in}$. Therefore, further theoretical studies are desirable to understand the behavior of real quasi-2D magnets in magnetic field.

ACKNOWLEDGMENTS

We would like to thank Dr. Ruggero Vaia for enlightening discussion concerning the field-induced Berezinskii-Kosterlitz-Thouless phase transition in the spatially anisotropic square lattice. The work was supported by VEGA Grant No. 1/0269/17 of the Scientific Grant Agency of

the Ministry of Education, Science, Research and Sport of the Slovak Republic and the Slovak Academy of Sciences, the Slovak Research and Development Agency Projects No. DS-2016-0046, No. APVV-0027-11, No. APVV-14-0078, and No. APVV-14-0073, and the Project No. ITMS 26220120047 of European Regional Development Fund. Part of the computing was performed in the High Performance Computing Center of the Matej Bel University in Banská Bystrica using the HPC infrastructure acquired in Projects No. ITMS 26230120002 and No. 26210120002. D.L. acknowledges projects "IT4Innovations National Supercomputing Center-LM2015070," "IT4Innovations excellence in science-LQ1602," and Student Grant Competitions of VSB-TU Ostrava SP2016/182.

[1] U. Schollwöck, J. Richter, D. J. J. Farnell, and R. F. Bishop, *Quantum Magnetism* (Springer, Berlin, 2004).
[2] J. V. José, *40 Years of Berezinskii-Kosterlitz-Thouless Theory* (World Scientific, London, 2013).
[3] J. Reuther and R. Thomale, Phys. Rev. B **83**, 024402 (2011).
[4] A. Ralko, M. Mambrini, and D. Poilblanc, Phys. Rev. B **80**, 184427 (2009).
[5] Anders W. Sandvik, Phys. Rev. Lett. **83**, 3069 (1999).
[6] D. Ihle, C. Schindelin, A. Weiße, and H. Fehske, Phys. Rev. B **60**, 9240 (1999).
[7] F.-J. Jiang, F. Kämpfer, and M. Nyfeler, Phys. Rev. B **80**, 033104 (2009).
[8] L. Siurakshina, D. Ihle, and R. Hayn, Phys. Rev. B **61**, 14601 (2000).
[9] Y. J. Kim and R. J. Birgeneau, Phys. Rev. B **62**, 6378 (2000).
[10] D. P. Landau and K. Binder, Phys. Rev. B **24**, 1391 (1981).
[11] A. R. Völkel, F. G. Mertens, A. R. Bishop, and G. M. Wysin, Phys. Rev. B **43**, 5992 (1991).
[12] A. Cuccoli, T. Roscilde, R. Vaia, and P. Verrucchi, Phys. Rev. Lett. **90**, 167205 (2003).
[13] A. Cuccoli, T. Roscilde, V. Tognetti, R. Vaia, and P. Verrucchi, Phys. Rev. B **67**, 104414 (2003).
[14] A. Cuccoli, T. Roscilde, R. Vaia, and P. Verrucchi, Phys. Rev. B **68**, 060402(R) (2003).
[15] H. Holtschneider and W. Selke, Eur. Phys. J. B **62**, 147 (2008).
[16] Chenggang Zhou, D. P. Landau, and T. C. Schulthess, Phys. Rev. B **74**, 064407 (2006).
[17] P. Sengupta, C. D. Batista, R. D. McDonald, S. Cox, J. Singleton, L. Huang, T. P. Papageorgiou, O. Ignatchik, T. Herrmannsdörfer, J. L. Manson, J. A. Schlueter, K. A. Funk, and J. Wosnitza, Phys. Rev. B **79**, 060409(R) (2009).
[18] V. Hinkov, P. Bourges, S. Pailhès, Y. Sidis, A. Ivanov, C. D. Frost, T. G. Perring, C. T. Lin, D. P. Chen, and B. Keimer, Nat. Phys. **3**, 780 (2007).
[19] B. C. Keith, C. P. Landee, T. Valleau, M. M. Turnbull, and N. Harrison, Phys. Rev. B **84**, 104442 (2011).
[20] R. Nath, M. Padmanabhan, S. Baby, A. Thirumurugan, D. Ehlers, M. Hemmida, H.-A. Krug von Nidda, and A. A. Tsirlin, Phys. Rev. B **91**, 054409 (2015).
[21] M. Kajňáková, M. Orendáč, A. Orendáčová, A. Vlček, J. Černák, O. V. Kravchyna, A. G. Anders, M. Bałanda, J.-H. Park, A. Feher, and M. W. Meisel, Phys. Rev. B **71**, 014435 (2005).
[22] R. Sýkora and D. Legut, J. Appl. Phys. **115**, 17B305 (2014).
[23] L. Baranová, A. Orendáčová, E. Čižmár, R. Tarasenko, V. Tkáč, M. Orendáč, and A. Feher, J. Magn. Magn. Mater. **404**, 53 (2016).
[24] R. Tarasenko, A. Orendáčová, E. Čižmár, S. Maťaš, M. Orendáč, I. Potočňák, K. Siemensmeyer, S. Zvyagin, J. Wosnitza, and A. Feher, Phys. Rev. B **87**, 174401 (2013).
[25] V. Manríqez, M. Campos-Valette, N. Lara, N. González-Tejeda, O. Wittke, G. Díaz, S. Diez, R. Muñoz, and L. Kriskovic, J. Chem. Crystallogr. **26**, 15 (1996).
[26] G. Kresse and J. Furthmüller, Phys. Rev. B **54**, 11169 (1996).
[27] J. P. Perdew, K. Burke, and M. Ernzerhof, Phys. Rev. Lett. **77**, 3865 (1996).
[28] S. L. Dudarev, G. A. Botton, S. Y. Savrasov, C. J. Humphreys, and A. P. Sutton, Phys. Rev. B **57**, 1505 (1998).
[29] A. W. Sandvik, Phys. Rev. B **59**, R14157(R) (1999).
[30] B. Bauer, L. D. Carr, H. G. Evertz, A. Feiguin, J. Freire, S. Fuchs, L. Gamper, J. Gukelberger, E. Gull, S. Guertler, A. Hehn, R. Igarashi, S. V. Isakov, D. Koop, P. N. Ma, P. Mates, H. Matsuo, O. Parcollet, G. Pawłowski, J. D. Picon, L. Pollet, E. Santos, V. W. Scarola, U. Schollwöck, C. Silva, B. Surer, S. Todo, S. Trebst, M. Troyer, M. L. Wall, P. Werner, and S. Wessel, J. Stat. Mech.: Theor. Exp. (2011) P05001.
[31] I. E. Dzyaloshinskii, Zh. Eksp. Teor. Fiz. **32**, 1547 (1957) [Sov. Phys.–JETP **5**, 1259 (1957)]; T. Moriya, Phys. Rev. Lett. **4**, 228 (1960).
[32] N. Papanicolaou, Phys. Rev. B **51**, 15062 (1995).
[33] K. Yu. Povarov, A. I. Smirnov, and C. P. Landee, Phys. Rev. B **87**, 214402 (2013).
[34] F. Xiao, F. M. Woodward, C. P. Landee, M. M. Turnbull, C. Mielke, N. Harrison, T. Lancaster, S. J. Blundell, P. J. Baker, P. Babkevich, and F. L. Pratt, Phys. Rev. B **79**, 134412 (2009).
[35] J. Liu, H.-J. Koo, H. Xiang, R. K. Kremer, and M.-H. Whangbo, J. Chem. Phys. **141**, 124113 (2014).
[36] H.-A. Krug von Nidda, L. E. Svistov, M. V. Eremin, R. M. Eremina, A. Loidl, V. Kataev, A. Validov, A. Prokofiev, and W. Aßmus, Phys. Rev. B **65**, 134445 (2002).
[37] S. Lebernegg, O. Janson, I. Rousochatzakis, S. Nishimoto, H. Rosner, and A. A. Tsirlin, Phys. Rev. B **95**, 035145 (2017).
[38] L. Sedláková, R. Tarasenko, I. Potočňák, A. Orendáčová, M. Kajňáková, M. Orendáč, V. A. Starodub, A. G. Anders, O. Kravchyna, and A. Feher, Solid State Commun. **147**, 239 (2008).
[39] P. Sengupta, A. W. Sandvik, and R. R. P. Singh, Phys. Rev. B **68**, 094423 (2003).
[40] S. Chakravarty, B. I. Halperin, and D. R. Nelson, Phys. Rev. Lett. **60**, 1057 (1988).
[41] A. R. Pereira and A. S. T. Pires, Phys. Rev. B **51**, 996 (1995).
[42] Y. Kohama, M. Jaime, O. E. Ayala-Valenzuela, R. D. McDonald, E. D. Mun, J. F. Corbey, and J. L. Manson, Phys. Rev. B **84**, 184402 (2011).
[43] L. J. de Jongh and A. R. Miedema, Adv. Phys. **23**, 1 (1974).
[44] T. Radu, H. Wilhelm, V. Yushankhai, D. Kovrizhin, R. Coldea, Z. Tylczynski, T. Lühmann, and F. Steglich, Phys. Rev. Lett. **95**, 127202 (2005).
[45] A. Cuccoli, G. Gori, R. Vaia, and P. Verruchi, J. Appl. Phys. **99**, 08H503 (2006).
[46] A. Orendáčová, Ber II Experimental Reports 2011/12, p. 22 (unpublished).